Chinese Chemical Letters 36 (2025) 110699

Contents lists available at ScienceDirect

Chinese Chemical Letters

journal homepage: www.elsevier.com/locate/cclet

Spatial-confinement combustion strategy enabling free radicals chemiluminescence direct-measurement in flame-retardant mechanism

Xuan Song, Teng Fu*, Yajie Yang, Yahan Kuang, Xiuli Wang, Yu-Zhong Wang*

The Collaborative Innovation Center for Eco-Friendly and Fire-Safety Polymeric Materials (MoE), National Engineering Laboratory of Eco-Friendly Polymeric Materials (Sichuan), State Key Laboratory of Polymer Materials Engineering, College of Chemistry, Sichuan University, Chengdu 610065, China

ARTICLE INFO

Article history:
Received 29 July 2024
Revised 25 November 2024
Accepted 28 November 2024
Available online 29 November 2024

Keywords:
Polymer combustion
Chain reaction
Radical chemiluminescence fingerprints
Flame separation
Flame retardant mechanism

ABSTRACT

Generally, gaining fundamental insights into chain processes during the combustion of flame-retardant polymers relies on the qualitative and quantitative characterization of key chain carriers. However, polymer combustion processes based on conventional solid-fuel combustion strategies, due to the high coupling of pyrolysis, combustion, soot formation and oxidation, exhibit relatively high complexity and poor flame stability, and lead to a huge obstacle to the use of optical diagnostics. Herein, a spatial-confinement combustion strategy, which can produce a special staged flame with multi-jets secondary wave, is devised to provide a highly decoupled combustion environment. Glowing soot particles are therefore decoupled from main chemiluminescence region and confined to the flame tip to provide a well-controlled, optical-thin test environment for combustion diagnostic. Based on this strategy, a multi-nozzle-separation (MNS) burner is designed and fabricated, and the combustion processes associated with four model compounds, PVC, PS, PP/TBBA blends and PP/RP blends are investigated by spontaneous spectral diagnosis, and the chemiluminescence fingerprint of key diatomic/triatomic intermediates (such as OH, CH, C_2, ClO, Br_2, and PHO) are clearly observed. This encouraging result means that the strategy of spatial-confinement combustion we proposed shows promising prospect in many subjects associated with combustion chain regulation, such as efficient design of flame retardants.

From the time attempts to conquer fire, human has never stopped studying combustion [1]. Particularly, the development of the general theory of branched-chain reactions marked a brand-new stage for combustion science [2]. Since then, combustion is commonly regarded as a kinetic mode of self-acceleration of a chemical process, which is a result of the progressively accelerated self-heating of the reaction system and the accelerating multiplication of chain carriers (mostly are active radicals, such as H, OH, CH, C_2) according to branched-chain avalanche [3]. On this basis, thermal and chemical effects of flame suppressants have been systematically investigated to open up new theories and practical options for effectively managing the processes of ignition, developing combustion (detonation), and extinction by controlling the branching and loss of chain carriers [4]. However, current studies mostly focus on combustion processes of gaseous reactants [5], and there has been little fundamental work reported on the burning of solids, especially for those widely-used organic polymers, despite the fact that it is of paramount importance in many aspects of daily life, such as energy utilization, materials synthesis, public security, and sustainable development [6–11].

Generally, gaining fundamental insights into chain processes relies on qualitative even quantitative characterization of key chain carriers [12]. Typically, using optical techniques, *in situ* and non-intrusive monitoring with high spatial and temporal resolution of active intermediates in combustion zones can be achieved. Yet, the potentially high sensitivity of combustion with respect to variations in physical boundary conditions can render measurement techniques under demanding combustion environments [13,14]. Therefore, experiments conducted in well-controlled, optically accessible environments are essential for such studies [15].

Polymer combustion based on conventional solid-fuel combustion strategies (entrained-flow gasifiers/combustor, drop-tube furnaces, and single-particle reactors, *etc.*), due to the high coupling of pyrolysis, combustion, soot formation and oxidation, exhibit relatively high complexity. Particularly, two distinctive features, solids pyrolysis and heterogeneous gas-solids reactions (especially for carbon oxidation), lead to a huge obstacle to the use of optical

* Corresponding authors.
E-mail addresses: futeng@scu.edu.cn (T. Fu), yzwang@scu.edu.cn (Y.-Z. Wang).

https://doi.org/10.1016/j.cclet.2024.110699
1001-8417/

techniques [16]. Specifically, (1) unlike gas/liquid fuel, polymers do not undergo self-sustaining chemical reactions after forced ignition (called as "self-extinguishing"). An external source (generally the gas flame) is essential to support sample pyrolysis and combustion chains, which, inevitably, cause strong interference to intermediates monitoring; (2) polymer flames produce substantial quantities of soot (indeed, the bright yellow luminescence occurring at the tip of most polymer flames is mainly due to blackbody radiation originated from soot oxidation), which largely reduces the measurability of reaction zone and leads to less effective or even complete failure for most optical techniques since the incandescence gives diffusion flame strong luminosity at the relevant wavelength [17–19].

To solve these problems, a spatial-confinement combustion strategy, which can produce a special staged flame with multi-jets secondary wave, is devised to provide a highly decoupled combustion environment. Briefly, a spatially-separated staged flame is used to provide the sufficient heat and chain initiators to maintain the continuous pyrolysis-combustion of polymer samples while ensuring minimal spectral interference. Furthermore, traditional cone-shaped secondary wave of the staged flame is altered into a cluster of micro jets, leading to a significant reduction in heterogeneous gas-solids reactions. Noteworthy, numerous literatures demonstrate that by altering the structure of diffusion flame to suppress soot inception, the luminous zone can be confined to the flame tip, and even a yellow sooting flame could change to a blue soot-free flame caused by radical chemiluminescence. Therefore, a well-controlled, optical-thin test environment for combustion diagnostic can be provided. Based on this strategy, a multi-nozzle-separation (MNS) burner is designed and fabricated, and the combustion processes associated with four model compounds, PVC (polyvinyl chloride), PS (polystyrene), PP/TBBA blends (polypropylene/tetrabromobisphenol A) and PP/RP blends (polypropylene/red phosphorus) are investigated by spontaneous spectral diagnosis (a passive optical diagnostic which is easily hindered in sooting flame), and the chemiluminescence fingerprint of key diatomic/triatomic intermediates (such as OH, CH, C_2, ClO, Br_2, and PHO) are clearly observed. This result indicates that the strategy of spatial-confinement combustion shows promising prospect in many subjects associated with combustion chain regulation, such as flame-retardant mechanism study.

MNS burner mainly includes a laminar flow burner and a home-built flame separator (called as "multi-nozzle separator"). As shown in Fig. 1a, the multi-nozzle separator is composed of an inner-outer-separation casing pipe which is used to separate the initial flame into the inner flame (Inner-F) and the "lift-off" outer flame (Outer-F) [20], and a multi-jet induced nozzle which is used to alter the Outer-F into a cluster of micro jets (a sample pool is inside the nozzle and directly above the Inner-F). Fig. 1b shows the digital image of the stable spatially-separated flame produced by MNS burner, where the Inner-F with intense greenish luminescence is the premix flame formed by the combustion of fuel (C_3H_8) and primary oxidants (O_2), and the pale bluish-violet Outer-F is the diffusion flame formed by the further combustion of incomplete-combustion products (according to previous study, mostly are CO and H_2) in atmospheric oxygen [21]. Fig. 1d and Fig. S1 (Supporting information) compare the relative emission intensity of the Initial-F (the flame produced by the laminar flow burner without the separator), Inner-F and Outer-F at the range of 200-1100 nm. The main bands of hydrocarbon flames, the 4315 Å system and 3900 Å system of CH (431 nm, $A^2\Delta \rightarrow X^2\pi$; 390 nm, $B^2\Sigma \rightarrow X^2$ [22]) and the Swan system of C_2 (473 nm, 516 nm, 558-563 nm, $A^3 \rightarrow X^3$ [22]), which can be clearly observed in the Initial-F and Inner-F, do not occur in the Outer-F. And a decrease in OH (3064 Å system, $A^2\Sigma^+ \rightarrow X^2$ [22]), CO_2 (carbon monoxide flame bands, $B_2 \rightarrow X^1\Sigma^+$ [22]) and H_2O (vibration-rotation bands [22]) chemiluminescence

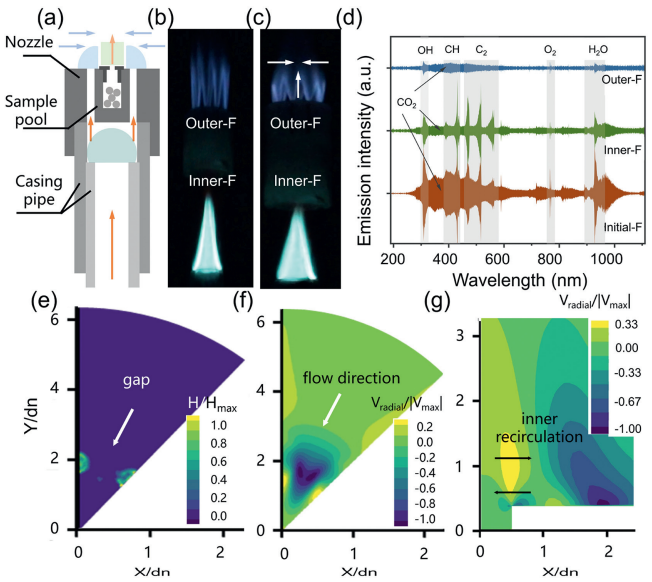

Fig. 1. Multi-nozzle separation burner. (a) Schematic diagram of the multi-nozzle separator and the spatially-separated flame. (b) Digital image of the spatially-separated flame before the pyrolysis of solid samples. (c) Digital image of the spatially-separated flame during the pyrolysis of solid samples (PP, ~350 °C). (d) Comparison of the emission intensity of Initial-F, Inner-F, and Outer-F. (e) Calculated H/H_{max} of the cross-section of the combustion zone. (f) Calculated $V_{radial}/|V_{max}|$ of the cross-section of combustion zone. (g) Calculated $V_{radial}/|V_{max}|$ of the longitudinal-section of the combustion zone.

intensity of over 1 orders of magnitude is observed in the Outer-F relative to the Initial-F. These results demonstrate that the Inner-F, retaining the most of active species and energy, is suitable for supporting sample pyrolysis. While the Outer-F, only showing faint luminescence, is a perfect candidate for combustion chain initiation due to the weak interference to the chemiluminescence of samples.

In addition, MNS Burner can effectively suppress the soot inception, thereby minimizing the interference of the luminous zone in flame tips. Generally, soot formation requires local carbon/oxygen (C/O) ratio to be above thresholds [23]. Where, in MNS burner, the local oxygen concentration can be enhanced by altering the flame structure of Outer-F. Specifically, as shown in Fig. 1c, several discrete flame sheets (NOT a continuous front) are formed at the top of MNS burner, and gaps between allow for the free flow of surrounding air into the Outer-F. Particularly, when samples start to pyrolysis, large numbers of volatile products are ejected from the sample cell, and accelerated as it flows through the circle nozzle with smaller diameter due to the Venturi effect. According to Bernoulli's principle, a low-pressure zone is formed on the top of the circle nozzle. Flame sheets are therefore gathering inwards to form a flame necking cone (Fig. 1c, noteworthy, the interaction between discrete flame fronts also plays an important role in forming this necking cone, but this behavior is reinforced and accentuated by the center jet and the combustion of volatile products), and the surrounding air is drawn into the Outer-F and mixed with volatile products thoroughly, leading to an increase in local oxygen concentration [24,25].

Numerical simulations are used to illustrate this process (see Note S1 in Supporting information for details) [26]. The normalized H mole fraction distributions of the cross-section of the combustion zone (H/H_{max}, generally, the spatial distribution of flame front can be characterized by the boundary of H distributions [27]. Fig. 1e and Fig. S2a (in Supporting information) demonstrate that the constituent flame sheets are isolated. And the normalized radial velocity distributions of the same plane (Fig. 1f and Fig. S2b in Supporting information, $V_{radial}/|V_{max}|$, the direction of air flow has

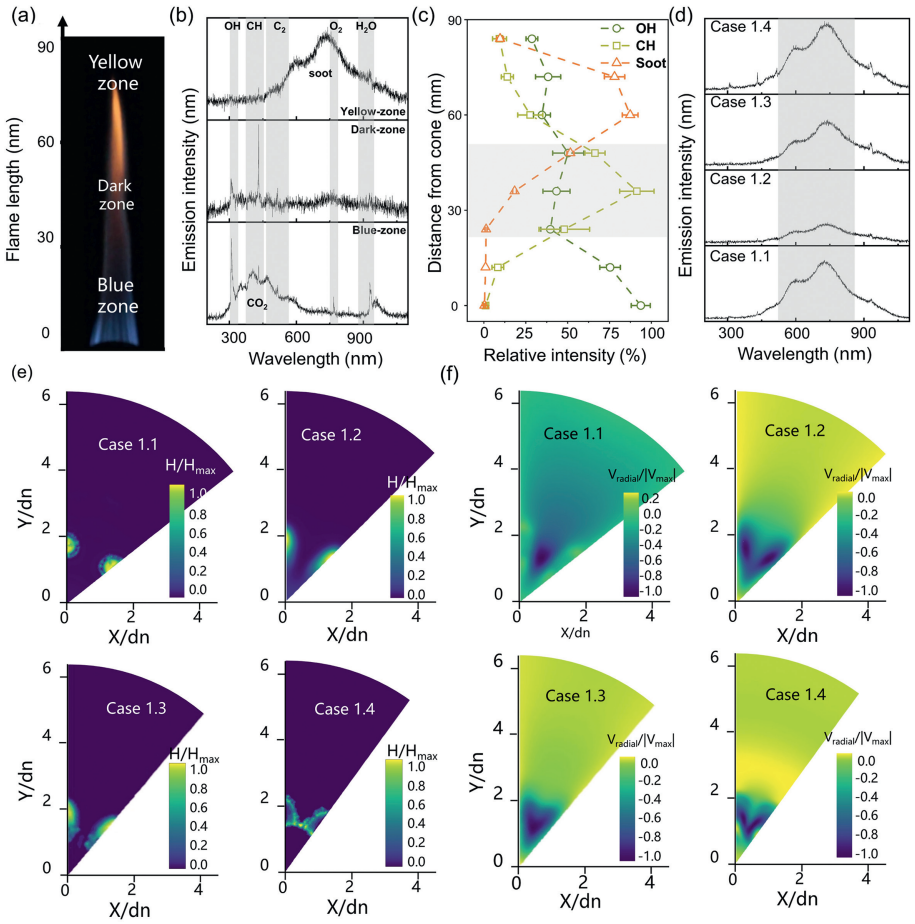

Fig. 2. Multi-nozzle jet to localized the soot inception. (a) Digital image of PP flame at around 400 °C. (b) Spectrogram of PP flame at around 400 °C. (c) Normalized emission intensity profiles of key intermediates and temperature profiles in PP flame. (d) The emission spectra under different cases. (e) Calculated H/H_{max} of the cross-section under different cases. (f) Calculated $V_{radial}/|V_{max}|$ of the cross-section under different cases.

been marked out) indicate that the external air is dragged into the Outer-F through the gaps between sheets. Noticeable, even under "before sample pyrolysis" (Fig. 1f), there is still inward air entrainment between flame sheets. This is because high-speed fuel jets can form low-pressure zones around the nozzle outlets and drag the surrounding air around the Outer-F, where a certain amount of air flows through gaps and reach the burner-axis due to the radial momentum. The longitudinal-section (Fig. 1g) clearly shows that a high-momentum-jet-induced gas recirculation zone is formed between two flame sheets. This recirculation zone plays an important role in soot suppression and flame stabilization since it can not only significantly improve the gas mixing efficiency to reduce local carbon content, but form a high-temperature zone to achieve the self-ignition of soot particles [28].

The effectiveness of MNS burner on soot suppression and soot confinement is then investigated. Fig. 2a records the digital images of PP (polypropylene, $(C_3H_6)_n$, one of the most commonly used thermoplastic) flame under "during sample pyrolysis" (~450 °C). It can be clearly seen that the PP flame produced by MNS burner is vertically-stretching-cone-shaped and can be divided into three zones by the color, the blue zone at the root, the dark zone in the middle and the bright-yellow zone at the top. Spectra tests (Fig. 2b) indicate that, compared to the Outer-F under "before sample pyrolysis" (Fig. 1b), blue zone shows almost the same spectral structure. This demonstrates that the blue zone is likely dominated by the diffusive and convective transport processes. In this region, a large amount of surrounding air is drawn into the Outer-F due to the effect of the high-speed center jet, followed by an intense mix with volatile products, which do not undergo the appreciable oxidation due to the relatively low temperature and short residence time (for the low molecular weight pyrolysis fragments) [29]. In the dark zone, the strongest features of hydrocarbon flames, CH and C_2, are clearly observed, which means the oxidation of pyrolysis products mostly occurs in this region. For the bright-yellow zone, the continuous emission band (due to the thermal radiation of hot carbon particles) [30] demonstrates that soot is formed and further oxidized in this zone. The normalized emission intensity profiles of key intermediates and temperature profiles in Fig. 2c indicate that PP flame produced by MNS burner can be characterized by the typical partially premixed flame [31], where a preheat zone at the root (blue zone), a reaction zone in the middle (dark zone), and a soot zone in the top (bright-yellow zone). Namely, the soot formation is localized in the flame tip and spatially separated from the region where key intermediates occur.

According to previous studies, mixing efficiency (soot formation) in multi-jet flames is highly related to the air entrainment, which determined by the interaction of flame sheets and primarily controlled by the distance between fuel jets [32]. To obtain the optimal soot suppression, separators with different numbers of fuel nozzles are built and tested. Fig. S3 (Supporting information) records the digital images of PP flames under separators with 7 (case 1.1), 8 (case 1.2), 9 (case 1.3) and 10 (case 1.4) nozzles at the same pyrolysis temperature (separators with fewer nozzles are not able to form stable staged flame, while more nozzles lead the continuous flame front). Obviously, the size of the yellow zone at the flame tip varies significantly with different numbers of nozzles,

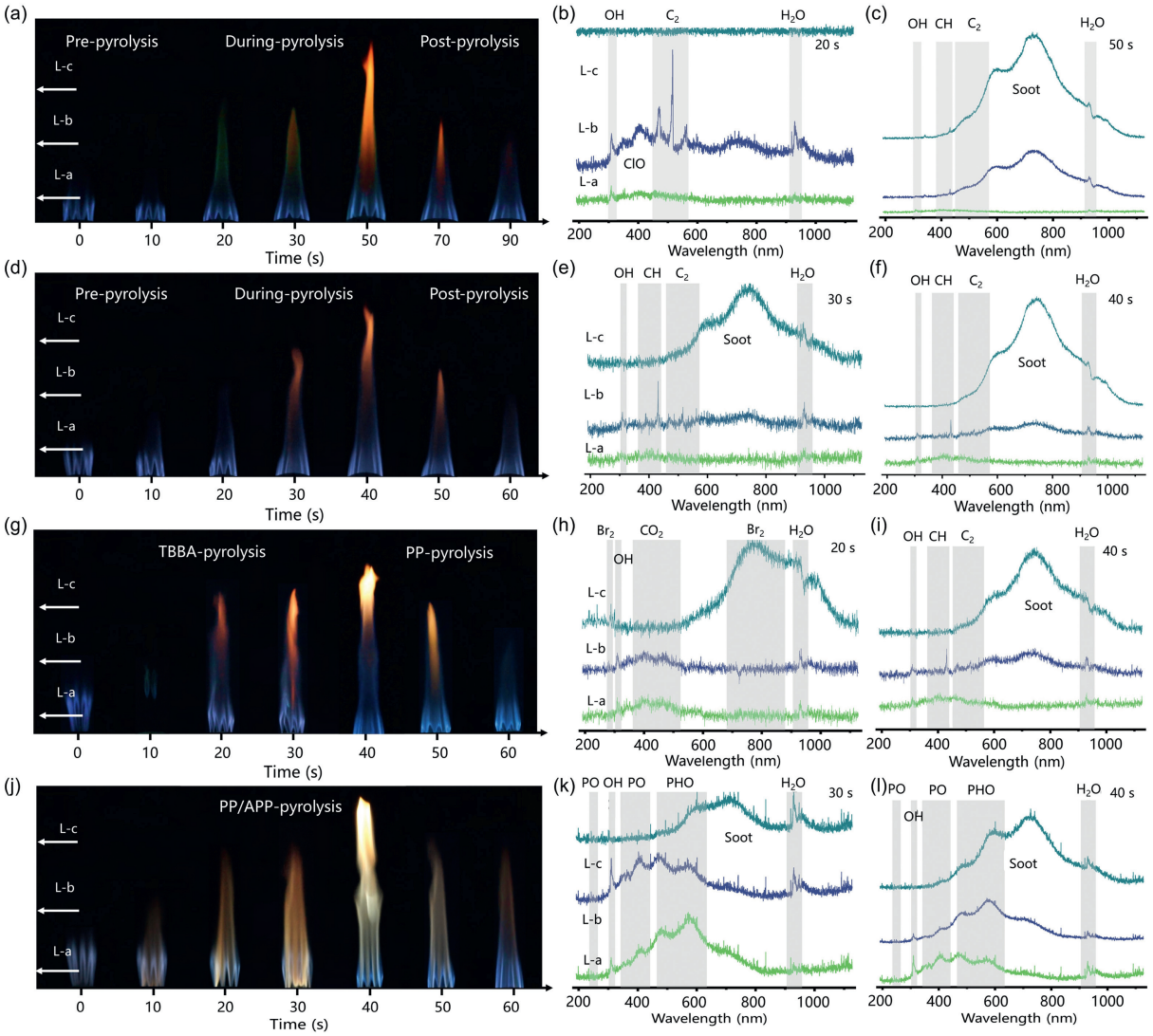

Fig. 3. The combustion processes of model compounds. (a) Digital images of PVC flames during the whole combustion process. (b) Spectrograms of the PVC flame at 20 s. (c) Spectrograms of the PVC flame at 50 s. (d) Digital images of PS flames during the whole combustion process. (e) Spectrograms of the PS flame at 30 s. (f) Spectrograms of the PS flame at 40 s. (g) Digital images of PP/TBBA flames during the whole combustion process. (h) Spectrograms of the PP/TBBA flame at 20 s. (i) Spectrograms of the PP/TBBA flame at 40 s. (j) Digital images of PP/RP flames during the whole combustion process. (k) Spectrograms of the PP/RP flame at 30 s. (l) Spectrograms of the PP/RP flame at 40 s.

and case 1.2 exhibits the smallest yellow zone, and also the most effective soot confinement. Fig. 2d shows the spectrograms of PP flames under different cases, where case 1.2 exhibits the weakest emission, further confirm the above results.

Numerical simulations are used to capture the detailed flow fields information to explain the variation in soot concentration under different cases. Fig. 2e (case 1.1) compares the H/H_{max} distributions of the cross-section of preheat zone under different cases. It is evident that with increasing nozzle numbers, the gaps between flame sheets gradually narrow. Particularly, for case 1.4, the flame fronts almost merge together and the access to oxygen is highly curtailed, leading to the highest soot loading. The radial velocity distributions in Fig. 2f indicate that, from 7 nozzles to 9 nozzles, the flow rate of the inward air gradually increases, leading to a higher shearing of the pyrolysis-product jet by the cross flow, and consequent a higher mixing efficiency. The soot formation is suppressed since the increased flow rate and mixing uniformity shorten the residence time for fuel pyrolysis and polycyclic aromatic hydrocarbons (PAHs) growth (collision and cluster formation) [33]. This explains the soot radiation in cases 1.2 and 1.3 are lower than case 1.1. In summary, based on results from experiments and numerical simulations, the separator with 8 nozzles is chosen for subsequent studies.

The combustion processes of four model compounds, PVC, PS, PP/TBBA blends and PP/RP blends are investigated, and the digital images and emission spectra are recorded to demonstrate the feasibility of our strategy.

Fig. 3a records the digital images of PVC flames during the whole combustion process. At first, only the pale bluish-violet secondary wave of the auxiliary flame can be observed in the preheat zone. When heating to around 300 °C (~20 s), the flame becomes unstable with a slightly increase in length, accompanied by noticeable green glowing in the reaction zone. In the meantime, spectral tests (Fig. 3b) capture a series of band spectra in this green flame, where, the two with heads respectively located at around 430 nm (degrade to the violet) and 390 nm (degrade to the red) are assigned to the 4315 Å system ($A^2\Delta \rightarrow X^2\pi$) and 3900 Å system ($B^2\Sigma \rightarrow X^2$) of CH. And the band system, which has three single heads located at around 473 nm, 516 nm and 560 nm (both degrade to the violet), is ascribed to the Swan system of C_2

($A^3 \rightarrow X^3$). In addition, the *pseudo*-continuous band system extending from around 360 nm to 450 nm, which possesses rather complex bands degraded to the red, is attributed to the emission of ClO ($A^2 \rightarrow X^2$ [34]). Further heating to around 450 °C (~40 s) leads another increase in length and a strong yellow luminesce occurs at the top of combustion zone. The spectrogram in Fig. 3c indicates that this yellow flame is due to the continuous band spanning from 600 nm to 800 nm, which is originated from the thermal radiation of soot particles. This unique change in flames is likely due to the special pyrolysis mechanism of PVC, which consists of two main degradation stages, dehydrochlorination and hydrocarbons release [35]. Where, the flame at around 250 °C is supported by the HCl/chlorinated hydrocarbons, while the yellow flame is due to the hydrocarbon oxidation.

For PS, as shown in Fig. 3d, the flame becomes oscillating with a slight increase in length at around 400 °C (~30 s), and in the meantime, a yellow luminescence region occurs in the flame tip. Spectrograms in Fig. 3e show that the characteristic bands of OH, CH, C_2, H_2O, and a relatively weak continuous emission band originate from the thermal radiation of soot particles are clearly observed. Further heating (~40 s, Fig. 3f) leads to a quick increase in flame length, and the luminescence region is significantly expanded. This result shows that at this moment a large amounts of hydrocarbon fuel are into the combustion zone, leading to a quick increase in local carbon-to-oxygen ratio and therefore significant soot formation.

For PP/TBBA, as shown in Fig. 3g, the flame becomes oscillating at around 300 °C (~20 s), accompanied by the characteristic orange-red glowing in the reaction zone. The spectrogram in Fig. 3h indicate that it is mainly due to the broad continuous band extending from around 510 nm to the near infrared (NIR), which is ascribed to the Orange-red system of Br_2 ($B^1 \rightarrow X^1\Sigma$, $A^3 \rightarrow X^1\Sigma$ [34]) and originated from the association of normal and excited halogen atom (*e.g.*, $Br + Br = Br_2 + h\nu$) [36]. Further heating (above 400 °C, ~30 s) leads a significant increase in flame length and turns the weak orange-red glowing to the bright yellow luminesce (Fig. 3i shows the spectrogram), demonstrating the occurrence of soot particles. This temperature-dependent flame can be explained by the TGA (thermogravimetry) curve of PP/TBBA (Fig. S4 in Supporting information), where the orange-red flame is due to the combustion of bromine-containing compound from the first weight-loss, while the soot flame is due to the combustion of pyrolysis products of PP and complete disintegration products of TBBA (such as benzene, toluene) [37].

For PP/RP, as shown in Fig. 3j, when heating to around 300 °C (~20 s), the pale bluish flame gradually turns to blue-yellow accompanied by a rapid increase in length. The spectrogram in Fig. 3k shows there are one clear band systems located at around 450-670 nm in the blue-yellow zone, which, according to previous studies, is probably originated from the emission of PHO (480-640 nm [34]). Deserve to mention that this band is very complex and apparently diffuse due to the relatively high temperature of the combustion zone (Studies by Lam Thanh and Peyron have proved that the higher temperature makes the structure of PHO more complex and diffuse.) [22]. Further heating (400 °C, ~40 s) lead to a brighter flame and a significant increase in emission intensity of the continues band at around 600-800 nm (Fig. 3l), which apparently attribute to the oxidation of solid particles. Noticeable, the structure of this continua is slightly different from the one observed in the combustion of pure PP (Fig. 2b). According to previous studies, this is possibly because the solid particles in the gas phase may include not only carbon soot, but those associated with phosphorus, such as P_2O_5 and P_2O_3.

Taken together, these results indicate that our strategy can significantly improve the optical transparency of combustion zone, and the characteristic chemiluminescence of key intermediates can be easily captured. Particularly, in our experiments, it has been proved that even the simplest emission spectroscopy, which is generally highly susceptible to background/soot interference and recognized as possessing relatively poor spatiotemporal-resolution, shows appealing results. We believe that by improving the optical monitoring module (replaced by some laser optical diagnostics), it will show more attractive results and broader application prospect.

In conclusion, by physically separating the interference term from reaction zone, an *in-situ*, nonintrusive intermediates monitoring method for polymer combustion mechanism study, is proposed. Based on this strategy, a special burner called MNS burner, which can not only realize continuous pyrolysis and combustion of polymers, but reduce the interference of background and thermal radiation, is designed and tested. Four model compounds, including polymer and additives which have a significant effect on combustion chain, have been investigated to prove the feasibility of this method. In particular, by qualitative or semi-quantitative monitoring of key radicals (OH, CH, C_2, H_2O, ClO, Br_2, PHO, *etc.*) in the combustion zone, this method can provide key evidence for the investigation of solid combustion/flame retardant mechanisms. Further works are in progress to explore the detailed mechanism and kinetics.

Declaration of competing interest

The authors declare that they have no known competing financial interests or personal relationships that could have appeared to influence the work reported in this paper.

CRediT authorship contribution statement

Xuan Song: Writing – review & editing, Writing – original draft, Methodology, Investigation, Formal analysis, Conceptualization. **Teng Fu:** Writing – review & editing, Writing – original draft, Conceptualization. **Yajie Yang:** Investigation. **Yahan Kuang:** Investigation. **Xiuli Wang:** Writing – original draft. **Yu-Zhong Wang:** Writing – review & editing, Writing – original draft, Investigation, Funding acquisition, Conceptualization.

Acknowledgments

This work was financially supported by the National Natural Science Foundation of China (No. 51827803), the Fundamental Research Funds for the Central Universities, 111 Center (No. B20001) and Institutional Research Fund from Sichuan University (No. 2021SCUNL201).

Supplementary materials

Supplementary material associated with this article can be found, in the online version, at doi:10.1016/j.cclet.2024.110699.

References

[1] S.J. Pyne, Fire: A Brief History, University of Washington Press, Seattle, 2019.
[2] L.A. Lovachev, Combust. Flame 4 (1960) 357–367.
[3] F.A. Williams, Combustion Theory, CRC Press, Boca Raton, 2018.
[4] Z. Wang, L. Zhang, K. Moshammer, et al., Combust. Flame 164 (2016) 386–396.
[5] S. McAllister, J.Y. Chen, A.C. Fernandez-Pello, Fundamentals of Combustion Processes, Springer, New York, 2011.
[6] B.W. Liu, H.B. Zhao, Y.Z. Wang, Adv. Mater. 34 (2022) 2107905.
[7] S. Xu, Y. Han, C. Zhou, et al., Chin. Chem. Lett. 34 (2023) 107202.
[8] X. Song, Z.P. Deng, C.B. Li, et al., Chin. Chem. Lett. 33 (2022) 4912–4917.
[9] S.Y. Zhang, T. Fu, Y. Gong, et al., Chin. Chem. Lett. 34 (2023) 107615.
[10] E.R. Kipp, J. Garcia-Barriocanal, A. Bhan, Angew. Chem. Int. Ed. 63 (2024) e202412932.

[11] Y.T. Yan, G. Wu, S.C. Chen, Y.Z. Wang, Chin. Chem. Lett. 33 (2022) 2151–2154.
[12] L. Chen, X. Qi, J. Tang, H. Xin, Z. Liang, Fuel 293 (2022) 120436.
[13] W. Sun, W. Zeng, L. Guo, et al., Fuel 349 (2023) 128507.
[14] M. Aldén, Proc. Combust. Inst. 39 (2023) 1185–1228.
[15] M. Aldén, J. Bood, Z. Li, M.J. Richter, Combust. Inst. 33 (2011) 69–97.
[16] D. Tillman, The Combustion of Solid Fuels And Wastes, Academic Press, Salt Lake City, 2012.
[17] Y. Xu, J. Zhu, X. Liu, et al., Fuel 312 (2002) 122948.
[18] I.J. Jagoda, G. Prado, J.J. Lahaye, Combust. Flame 37 (1980) 261–274.
[19] J. Zhang, C. Schulze-Netzer, T. Li, T. Løvås, Proc. Combust. Inst. 40 (2024) 105575.
[20] M. Nishioka, Y. Ishigami, H. Horii, Y. Umeda, Y. Nakamura, Combust. Flame 147 (2006) 93–107.
[21] J. Wang, W. Fan, Y. Li, et al., Energy 37 (2012) 725–736.
[22] A. Gaydon, The Spectroscopy of Flames, Springer, New York, 2012.
[23] J. Morán, A. Poux, F. Cepeda, et al., Combust. Flame 256 (2023) 112987.
[24] Z. Liu, Y. Xiong, Z. Zhang, et al., Fuel 327 (2022) 125138.
[25] A. Durocher, L. Fan, M. Füri, et al., Proc. Combust. Inst. 40 (2024) 105561.
[26] H. Li, J. Zhang, G. Xie, Y. Lou, Z. Zhou, Appl. Therm. Eng. 235 (2023) 121271.
[27] D. Yu, Z. Chen, Prog. Energy Combust. Sci. 104 (2024) 101174.
[28] M. Thomson, T. Mitra, Science 361 (2018) 978–979.
[29] M.J. Thomson, Prog. Energy Combust. Sci. 39 (2023) 805–823.
[30] Z. Li, C. Lou, B.M. Kumfer, Combust. Flame 245 (2022) 112335.
[31] R. Sadanandan, J. Brunzendorf, M. Paul, H. Grosshans, D. Markus, Combust. Sci. Technol. 194 (2022) 1091–1107.
[32] M. Bouvier, G. Cabot, J. Yon, F. Grisch, Proc. Combust. Inst. 38 (2021) 1851–1858.
[33] A.K. Lemmens, D.B. Rap, J.M. Thunnissen, B. Willemsen, A.M. Rijs, Nat. Commun. 11 (2022) 269.
[34] R.W.B. Pearse, A.G. Gaydon, The Identification of Molecular Spectra, Chapman and Hall, London, 1976.
[35] Z. Xu, S.S. Kolapkar, S. Zinchik, E. Bar-Ziv, A.G. McDonald, Polym. Degrad. Stab. 176 (2020) 109148.
[36] M. Clyne, J.A. Coxon, J. Mol. Spectrosc. 23 (1967) 258–271.
[37] K.H. Zhang, L.J. Bao, Y. Wang, H.M. Yang, Y. Gao, J. Hazard. Mater. 474 (2024) 134806.